Engineering Fracture Mechanics 219 (2019) 106547

Contents lists available at ScienceDirect

Engineering Fracture Mechanics

journal homepage: www.elsevier.com/locate/engfracmech

Semi-analytical approach for torsion problems of a circular bar containing multiple holes and/or cracks

Ying-Te Lee[a,*], Jeng-Tzong Chen[a,b,c,d], Shyh-Rong Kuo[a]

[a] Department of Harbor and River Engineering, National Taiwan Ocean University, Keelung, Taiwan
[b] Department of Mechanical and Mechatronic Engineering, National Taiwan Ocean University, Keelung, Taiwan
[c] Department of Civil Engineering, National Cheng Kung University, Tainan, Taiwan
[d] Center of Excellence for Ocean Engineering, National Taiwan Ocean University, Keelung, Taiwan

ARTICLE INFO

Keywords:
Torsional rigidity
Stress intensity factor
Degenerate kernel
Warping function
Crack

ABSTRACT

A semi-analytical approach of the null-field integral equation in conjunction containing the degenerate kernels is used to deal with the torsion problems of a circular bar with circular or elliptic holes and/or line cracks. In order to fully capture the elliptic geometry, the use of the addition theorem in terms of the elliptic coordinates plays an important role to expand the fundamental solution into the degenerate form. The boundary densities are expressed by using the eigenfunction expansion for the elliptic boundary. It is worthy of noting that the model of elliptic hole in companion with the limiting process of approaching the length of the semi-minor axis to zero is adopted to simulate the line crack. Besides, we also make the length of the semi-major axis close to the length of the semi-minor axis to approximate the circular boundary. By collocating the observation point exactly on the real boundary and matching the boundary conditions, a linear algebraic system is easily constructed to determine the unknown eigenfucntion coefficients. This approach can be seen as a semi-analytical manner since error purely attributes to the truncation of eigenfunction expansions and the convergence rate of exponential order is better than the linear order of the conventional boundary element method. Finally, several numerical examples of a circular bar with circular or elliptic holes and/or line cracks are employed to show the validity of the proposed approach. Not only the torsional rigidity but also the stress intensity factors are calculated to compare with the available results in the literature.

1. Introduction

The torsion problems can be found in many engineering practices such as screw, bolt, drive shaft, propeller shaft, etc. In order to reduce the weight of the structure or to save materials, cylindrical holes usually exist in the torsion bar such as circular or elliptical cylindrical holes due to easily making. Besides, some defects like cracks sometimes exist in the devices. Therefore, studying the stress distribution or material strength of a torsion bar with holes and/or cracks becomes important and meaningful issues.

The torsion problem can be traced back to the nineteenth century. The French scientist, Saint Venant, first proposed the classical Saint-Venant torsion problem. After that, many researchers paid their attention on studying torsion problems. Based on the Saint-Venant torsion theory, Ling [1] solved the torsion problem of a circular bar with longitudinal circular holes of equal radii distributed uniformly in a ring. Muskhelishvili [2] solved the problem of a circular bar reinforced by an eccentric circular inclusion. Chen and

* Corresponding author.
E-mail addresses: ytlee@mail.ntou.edu.tw (Y.-T. Lee), jtchen@mail.ntou.edu.tw (J.-T. Chen), srkuo@mail.ntou.edu.tw (S.-R. Kuo).

https://doi.org/10.1016/j.engfracmech.2019.106547
Received 12 April 2019; Received in revised form 1 July 2019; Accepted 7 July 2019
Available online 09 July 2019

Weng [3] have introduced conformal mapping with a Laurent series expansion to analyze the Saint-Venant torsion problem. They concerned on an eccentric bar of different materials with an imperfect interface under torque. Since the conformal mapping is limited to the doubly-connected region, it encounters difficulty for solving the problem with multiple inclusions. Therefore, many researchers paid more attentions on developing numerical methods or other techniques. In 1983, Caulk [4] developed a special boundary integral method to deal with the problem of a torsion bar with circular holes. Katsikadelis and Sapountzakis [5] used the boundary element method to solve the problem of an elliptic bar including one and two elliptic inclusions. Also, a practical problem of a rectangular concrete containing a Steel-I beam was concerned in their research. Later, Sapountzakis and Mokos [6–8] extended to deal with the nonuniform torsion problem that the composite bar is subject to an arbitrarily concentrated or distributed twisting moment. Shams-Ahmadi and Chou [9] used the complex variable boundary element method (CVBEM) to solve the torsion problem of composite shafts with arbitrary number of inclusions of different materials. Ang and Kang [10] developed a general formulation for solving the second-order elliptic partial differential equation for a multiply-connected region in a different version of CVBEM. Petrov [11] developed an effective technique of boundary element method (BEM) to determine torsion, shear and other characteristics of beam cross-sections of arbitrary complex shape including multiply-connected cross sections. However, these works are limited on studying a torsion bar with holes or inclusions instead of cracks.

For the problem of a torsion bar with cracks, Sih [12] employed the conformal mapping and complex variable theory to develop a self-contained method in connection with the Griffith-Irwin theory of fracture to find the stress solutions in a cracked body with longitudinal shear. Tang [13] utilized the singular and hypersigular formulations to solve a series of torsion problems with holes, inclusions and/or cracks. Based on the Saint-Venant torsion theory, Yue and Tang [14] proposed a linear inclusion model for torsion problems. They used the Mellin transform to obtain the fundamental solution of a single inclusion and combined this fundamental solution with the solution of a single crack and the single-layer potential function to obtain the torsional function for a torsion bar with inclusions and cracks. Wang and Lu [15] applied the boundary element method to solve the torsion problem of a circular bar with curvilinear cracks. Later, Lu and his coworkers [16] extended to deal with elliptical and rectangular torsion bars with curvilinear cracks. Based on the complex variable method, Huang and Gao [17] applied the Faber series expansion, Fourier series expansion and conformal mappings to propose a semi-analytical method for calculating the shear stresses and torsional rigidity of a circular shaft containing multiple holes or cracks.

Recently, meshless methods [18,19] become very popular, since it is free of mesh generation and only nodes are needed. The present formulation can be seen as one kind of meshless methods, since only observation points on the real boundary are required to satisfy the boundary condition. In Caulk's paper [4], he pointed out that Ling's result of three holes deviated from his data. Chen et al. [20] supported the Caulk's comment by using the null-field integral approach. On the other hand, Bird and Steele [21] found the discrepancy between the Naghdi's solution [22] and their data for the beam bending problem with four holes. Also, Chen and Chen's results [23] agreed with the Naghdi's results. Chen and Lee [24] used the null-field integral equation in conjunction with the degenerate kernel to solve a circular composite bar with circular inclusions. They found that their results were different from those of Kuo and Conway [25], but were the same as the data of FE solution obtained by Murakami and Yamakawa [26]. Later, they [27] also extended their approach to solve an elliptic torsion bar with elliptical inclusions. However, the problems that have been successfully solved are focused on the problems containing circular or elliptic boundaries. Following the successful experiences of [24,27], we extend the approach to solve torsion problems with holes and/or cracks.

In this paper, a semi-analytical approach is utilized to solve the Saint-Venant torsion problem of a circular bar with multiple holes and/or cracks. The mathematical tools, the degenerate kernel for the fundamental solution and eigenfuncion expansion for the boundary density, are used in the null-field integral formulation. In our approach, the model of elliptic hole in companion with the limiting process of approaching the length of semi-minor axis to zero is adopted to simulate the line cracks. By collocating the null-field point exactly on the real boundary and matching the boundary condition, the linear algebraic system can be easily constructed to determine the unknown coefficients of eigenfunction expansion. Then, the warping function, torsional rigidity and stress intensity factor can be obtained by the developed program. Finally, several numerical examples are given to show the validity and efficiency of the proposed approach.

2. Problem statement and formulation

2.1. Problem statement

A circular bar containing circular and elliptic holes and cracks bounded to the contours B_k ($k = 0,\ 1,\ 2,\ \cdots, N$) is shown in Fig. 1. We define

$$B = \bigcup_{k=0}^{N} B_k. \tag{1}$$

The circular bar twisted by couples applied at the end is taken into consideration. Following the theory of Saint-Venant torsion [28], we assume the displacement to be

$$u = -\alpha y z, \quad v = \alpha x z, \quad w = \alpha \varphi(x, y), \tag{2}$$

where α is the angle of twist per unit length along the z direction and φ is the warping function. The relation of strain and displacement is defined in the elasticity book [28] as shown below:

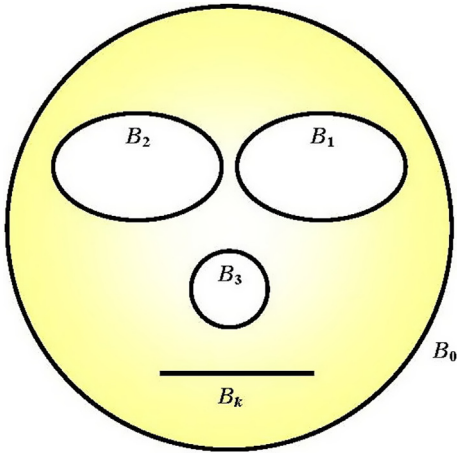

Fig. 1. Sketch of a circular bar containing circular and elliptic holes and cracks.

$$\begin{aligned}
\varepsilon_x &= \frac{\partial u}{\partial x}, \quad \gamma_{xy} = \frac{\partial u}{\partial y} + \frac{\partial v}{\partial x}, \\
\varepsilon_y &= \frac{\partial v}{\partial y}, \quad \gamma_{yz} = \frac{\partial v}{\partial z} + \frac{\partial w}{\partial y}, \\
\varepsilon_z &= \frac{\partial w}{\partial z}, \quad \gamma_{zx} = \frac{\partial w}{\partial x} + \frac{\partial u}{\partial z}.
\end{aligned} \tag{3}$$

Then, substituting the displacement of Eq. (2) into Eq. (3), we have the strain components as follows:

$$\begin{aligned}
&\varepsilon_x = \varepsilon_y = \varepsilon_z = \gamma_{xy} = 0, \\
&\gamma_{xz} = \alpha\left(\frac{\partial \varphi}{\partial x} - y\right), \\
&\gamma_{yz} = \alpha\left(\frac{\partial \varphi}{\partial y} + x\right).
\end{aligned} \tag{4}$$

By applying the Hooke's law, the stress components are

$$\begin{aligned}
&\sigma_x = \sigma_y = \sigma_z = \sigma_{xy} = 0, \\
&\sigma_{xz} = \mu\alpha\left(\frac{\partial \varphi}{\partial x} - y\right), \\
&\sigma_{yz} = \mu\alpha\left(\frac{\partial \varphi}{\partial y} + x\right),
\end{aligned} \tag{5}$$

where μ is the shear modulus. There is no distortion in the planes of cross sections since $\varepsilon_x = \varepsilon_y = \varepsilon_z = \gamma_{xy} = 0$. We have the state of pure shear at each point defined by the stress components σ_{xz} and σ_{yz}. By substituting Eq. (5) to the equilibrium equations

$$\begin{aligned}
&\frac{\partial \sigma_x}{\partial x} + \frac{\partial \sigma_{xy}}{\partial y} + \frac{\partial \sigma_{xz}}{\partial z} + F_x = 0, \\
&\frac{\partial \sigma_y}{\partial y} + \frac{\partial \sigma_{xy}}{\partial x} + \frac{\partial \sigma_{yz}}{\partial z} + F_y = 0, \\
&\frac{\partial \sigma_z}{\partial z} + \frac{\partial \sigma_{xz}}{\partial x} + \frac{\partial \sigma_{yz}}{\partial y} + F_z = 0,
\end{aligned} \tag{6}$$

the warping function satisfies the Laplace equation

$$\frac{\partial^2 \varphi}{\partial x^2} + \frac{\partial^2 \varphi}{\partial y^2} = \nabla^2 \varphi = 0 \text{ in } D, \tag{7}$$

where the body forces (F_x, F_y and F_z) are neglected and D is the domain of interest. On the cylinder surface, the stress states in Eq. (5) result in zero traction of $t_x = t_y = 0$. The only nonzero traction is t_z. Since there is no external traction, t_z, on the cylindrical surface, we have

$$t_z = \sigma_{xz} n_x + \sigma_{yz} n_y = \mu\alpha\left(\frac{\partial \varphi}{\partial x} n_x + \frac{\partial \varphi}{\partial y} n_y - y n_x + x n_y\right) = 0. \tag{8}$$

Therefore, the parenthesis in Eq. (8) is equal to zero and we have the boundary condition as follows:

$$\frac{\partial \varphi}{\partial x} n_x + \frac{\partial \varphi}{\partial y} n_y = \nabla \varphi \cdot \mathbf{n} = \frac{\partial \varphi}{\partial n} = y n_x - x n_y. \tag{9}$$

2.2. Dual null-field boundary integral formulation

2.2.1. Conventional version

The integral equation for the domain point can be derived from the third Green's identity, we have

$$\varphi(\mathbf{x}) = \int_B T(\mathbf{s}, \mathbf{x})\varphi(\mathbf{s})dB(s) - \int_B U(\mathbf{s}, \mathbf{x})\psi(\mathbf{s})dB(\mathbf{s}), \quad \mathbf{x} \in \Omega, \tag{10}$$

$$\psi(\mathbf{x}) = \int_B M(\mathbf{s}, \mathbf{x})\varphi(\mathbf{s})dB(s) - \int_B L(\mathbf{s}, \mathbf{x})\psi(\mathbf{s})dB(\mathbf{s}), \quad \mathbf{x} \in \Omega, \tag{11}$$

where B is the boundary, $\mathbf{s}$ and $\mathbf{x}$ are position of the source and field points, respectively, $\psi(\mathbf{x}) = \frac{\partial\varphi(\mathbf{x})}{\partial\mathbf{n}_\mathbf{x}}$, $\psi(\mathbf{s}) = \frac{\partial\varphi(\mathbf{s})}{\partial\mathbf{n}_\mathbf{s}}$, $\mathbf{n}_\mathbf{s}$ and $\mathbf{n}_\mathbf{x}$ denote the outward normal vectors at the source point $\mathbf{s}$ and field point $\mathbf{x}$, respectively, Ω is the domain of interest and the kernel function, $U(\mathbf{s}, \mathbf{x}) = \frac{1}{2\pi}\ln r$ ($r \equiv |\mathbf{x} - \mathbf{s}|$), is the fundamental solution which satisfies

$$\nabla^2 U(\mathbf{s}, \mathbf{x}) = \delta(\mathbf{x} - \mathbf{s}), \tag{12}$$

in which $\delta(\mathbf{x} - \mathbf{s})$ denotes the Dirac-delta function. The other kernel functions, $T(\mathbf{s}, \mathbf{x})$, $L(\mathbf{s}, \mathbf{x})$, and $M(\mathbf{s}, \mathbf{x})$, are defined by

$$\begin{aligned} T(\mathbf{s}, \mathbf{x}) &= \frac{\partial U(\mathbf{s}, \mathbf{x})}{\partial \mathbf{n}_\mathbf{s}}, \\ L(\mathbf{s}, \mathbf{x}) &= \frac{\partial U(\mathbf{s}, \mathbf{x})}{\partial \mathbf{n}_\mathbf{x}}, \\ M(\mathbf{s}, \mathbf{x}) &= \frac{\partial^2 U(\mathbf{s}, \mathbf{x})}{\partial \mathbf{n}_\mathbf{s}\partial \mathbf{n}_\mathbf{x}}. \end{aligned} \tag{13}$$

By moving the field point $\mathbf{x}$ to the boundary, the dual boundary integral equations for the boundary point can be obtained as follows:

$$\frac{1}{2}\varphi(\mathbf{x}) = C.P.V. \int_B T(\mathbf{s}, \mathbf{x})\varphi(\mathbf{s})dB(s) - \int_B U(\mathbf{s}, \mathbf{x})\psi(\mathbf{s})dB(\mathbf{s}), \quad \mathbf{x} \in B, \tag{14}$$

$$\frac{1}{2}\psi(\mathbf{x}) = H.P.V. \int_B M(\mathbf{s}, \mathbf{x})\varphi(\mathbf{s})dB(s) - C.P.V. \int_B L(\mathbf{s}, \mathbf{x})\psi(\mathbf{s})dB(\mathbf{s}), \quad \mathbf{x} \in B, \tag{15}$$

where *C.P.V.* and *H.P.V.* denote the Cauchy principal value and Hadamard (or called Mangler) principal value, respectively. Besides, once the field point $\mathbf{x}$ locates outside the domain ($\mathbf{x} \in \Omega^c$), we obtain the dual null-field integral equations as shown below

$$0 = \int_B T(\mathbf{s}, \mathbf{x})\varphi(\mathbf{s})dB(s) - \int_B U(\mathbf{s}, \mathbf{x})\psi(\mathbf{s})dB(\mathbf{s}), \quad \mathbf{x} \in \Omega^c, \tag{16}$$

$$0 = \int_B M(\mathbf{s}, \mathbf{x})\varphi(\mathbf{s})dB(s) - \int_B L(\mathbf{s}, \mathbf{x})\psi(\mathbf{s})dB(\mathbf{s}), \quad \mathbf{x} \in \Omega^c, \tag{17}$$

where Ω^c is the complement of a domain. Eqs. (10), (11), (16) and (17) are conventional formulations where the observation point is not located on the real boundary. Singularity occurs and concept of principal values is required once Eqs. (14) and (15) are considered. The traction $t(\mathbf{s})$ is the directional derivative of $u(\mathbf{s})$ along the outer normal direction at $\mathbf{s}$. In order to satisfy the interface condition, the observation points are located on the boundary. In the literature, many researchers used the integral equation for the domain point (Eqs. (10) and (11)) or the null-field integral equation (Eqs. (16) and (17)) combined with the so-called "bump contour" scheme as shown in Fig. 2 to determine the principal value. Therefore, the jump value $\left(\frac{\varphi}{2}, -\frac{\varphi}{2} \text{ or } -\frac{\psi}{2}\right)$ is determined. An alternative way to derive the jump value by using the complex variable method is proposed by Chen and Lin [29–31]. However, we do not calculate the principal value in the present approach and can make the observation point exactly locate on the real boundary not only including the null-field integral equation but also including the integral equation for the domain point. These two formulae can both contain the boundary point. The key point is that the degenerate kernel or the so-called separable kernel is introduced to replace the closed-form fundamental solutions in two sides of boundary. The detailed formulation is given in the next section. Besides, for

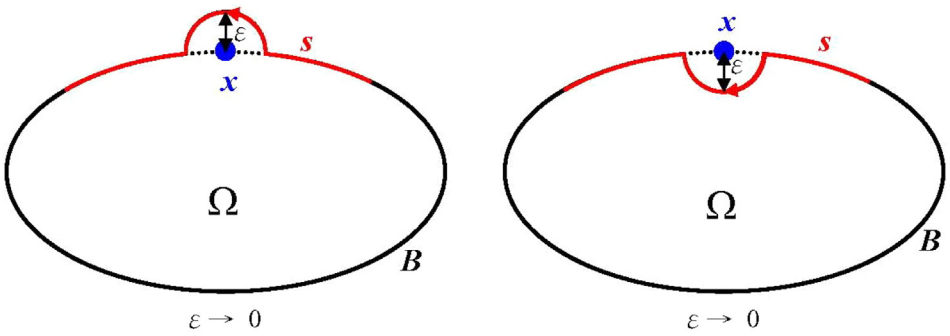

Fig. 2. The scheme of bump contour.

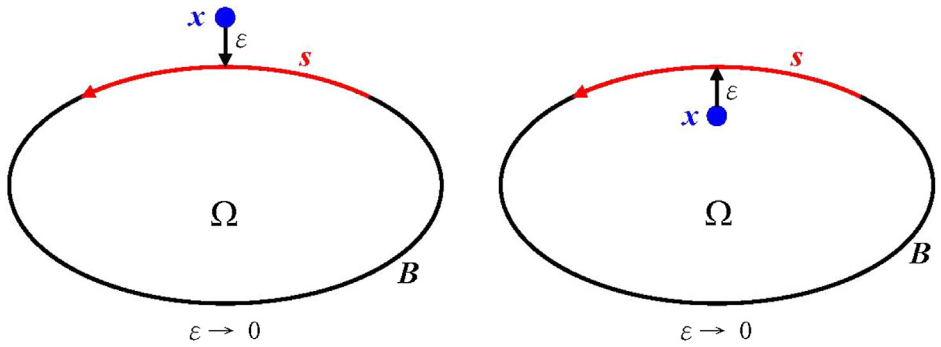

Fig. 3. Limiting process (present approach).

calculating the stress in the domain, the normal vector of an interior point is artificially given, *e.g.* $\psi(\mathbf{x}) = \frac{\partial\varphi(\mathbf{x})}{\partial x}$, if $\mathbf{n} = (1,\ 0)$ and $\psi(\mathbf{x}) = \frac{\partial\varphi(\mathbf{x})}{\partial y}$, if $\mathbf{n} = (0,\ 1)$. In other words, the selection of $\mathbf{n}$ depends on the stress under consideration.

2.2.2. The present version

By introducing the degenerate kernels, the observation point can be located on the real boundary free of calculating principal value using a small circular bump as shown in Fig. 3. Therefore, the representations of integral equations including the boundary point for the interior problem can be written as

$$\varphi(\mathbf{x}) = \int_B T^i(\mathbf{s},\mathbf{x})\varphi(\mathbf{s})dB(s) - \int_B U^i(\mathbf{s},\mathbf{x})\psi(\mathbf{s})dB(\mathbf{s}), \quad \mathbf{x}\in\Omega\cup B, \tag{18}$$

$$\psi(\mathbf{x}) = \int_B M^i(\mathbf{s},\mathbf{x})\varphi(\mathbf{s})dB(s) - \int_B L^i(\mathbf{s},\mathbf{x})\psi(\mathbf{s})dB(\mathbf{s}), \quad \mathbf{x}\in\Omega\cup B, \tag{19}$$

and

$$0 = \int_B T^e(\mathbf{s},\mathbf{x})\varphi(\mathbf{s})dB(s) - \int_B U^e(\mathbf{s},\mathbf{x})\psi(\mathbf{s})dB(\mathbf{s}), \quad \mathbf{x}\in\Omega^c\cup B, \tag{20}$$

$$0 = \int_B M^e(\mathbf{s},\mathbf{x})\varphi(\mathbf{s})dB(s) - \int_B L^e(\mathbf{s},\mathbf{x})\psi(\mathbf{s})dB(\mathbf{s}), \quad \mathbf{x}\in\Omega^c\cup B, \tag{21}$$

once the kernels are expressed in terms of an appropriate degenerate forms (denoted by subscripts i and e) instead of the closed-form fundamental solution. It is noted that $\mathbf{x}$ in Eqs. (18)–(21) can be exactly located on the real boundary.

For the exterior problem, the domain of interest (Ω) is in the external region of the elliptic boundary and the complement of a domain (Ω^c) is in the internal region of the ellipse. Therefore, the integral equation for the domain point and the null-field integral equations are, respectively, represented as

$$\varphi(\mathbf{x}) = \int_B T^e(\mathbf{s},\mathbf{x})\varphi(\mathbf{s})dB(s) - \int_B U^e(\mathbf{s},\mathbf{x})\psi(\mathbf{s})dB(\mathbf{s}), \quad \mathbf{x}\in\Omega\cup B, \tag{22}$$

$$\psi(\mathbf{x}) = \int_B M^e(\mathbf{s},\mathbf{x})\varphi(\mathbf{s})dB(s) - \int_B L^e(\mathbf{s},\mathbf{x})\psi(\mathbf{s})dB(\mathbf{s}), \quad \mathbf{x}\in\Omega\cup B, \tag{23}$$

and

$$0 = \int_B T^i(\mathbf{s},\mathbf{x})\varphi(\mathbf{s})dB(s) - \int_B U^i(\mathbf{s},\mathbf{x})\psi(\mathbf{s})dB(\mathbf{s}), \quad \mathbf{x}\in\Omega^c\cup B, \tag{24}$$

$$0 = \int_B M^i(\mathbf{s},\mathbf{x})\varphi(\mathbf{s})dB(s) - \int_B L^i(\mathbf{s},\mathbf{x})\psi(\mathbf{s})dB(\mathbf{s}), \quad \mathbf{x}\in\Omega^c\cup B, \tag{25}$$

Also, the observation point $\mathbf{x}$ in Eqs. (22)–(25) can be exactly located on the real boundary. For various problems (interior or exterior), we used different kernel functions (denoted by superscripts "i" and "e") so that the jump term $\left(\frac{\varphi}{2},\ -\frac{\varphi}{2},\ \frac{\psi}{2}\text{ or }-\frac{\psi}{2}\right)$ across boundary can be easily derived. Therefore, different expressions of the kernels for the interior and exterior observer points are used and they will be elaborated on later.

It is worthy of noting that our approach can yield the same linear algebraic equation derived from boundary integral equation in Eqs. (14) and (15). However, the procedure is quite different although observation points are located on the real boundary for both the conventional BIEM and the present approach. For the conventional BEM, it is necessary to calculate the singular or hypersingular integrals by using the sense of principal value. Our approach is free of calculating the principal value due to the introduction of the degenerate kernel since the kernel functions were separated into two parts, interior and exterior parts. If the appropriate kernels (interior and exterior parts) are chosen, we can easily obtain the same linear algebraic equation derived from the conventional BIE and free of calculating principal value.

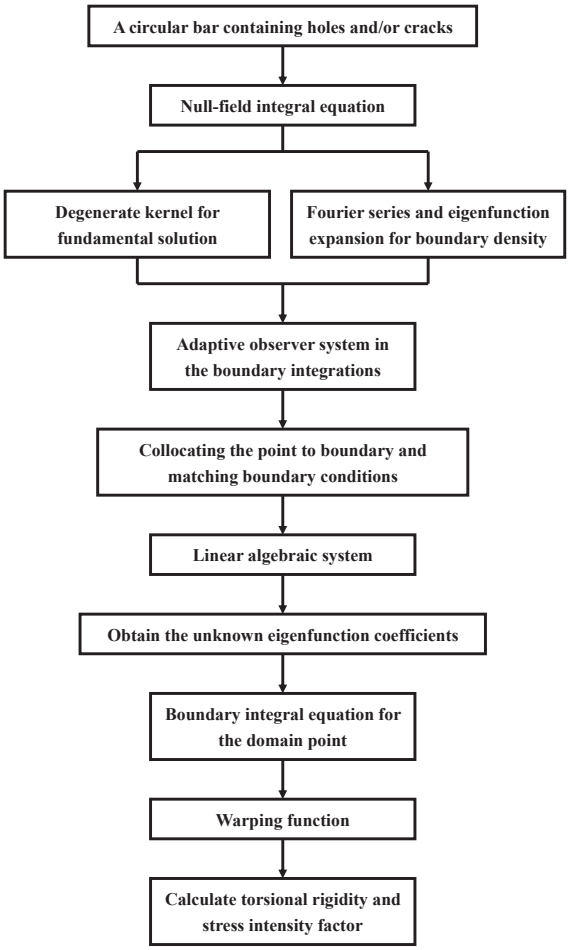

Fig. 4. Flowchart of the proposed approach.

2.2.3. Expansions of the fundamental solution and the boundary density

Based on the separable property, the kernel function $U(\mathbf{s}, \mathbf{x})$ can be expanded into degenerate form by employing the separating technique for source point and field point under the elliptic coordinates (ξ, η). The relation of the position vector represented in the Cartensian coordinates (x_1, x_2), (s_1, s_2) and in the elliptic coordinates (ξ, η), $(\bar{\xi}, \bar{\eta})$ is shown as follows:

$$\begin{aligned} &\mathbf{x} = (x_1, x_2) = (\xi, \eta) \quad \text{for the field point} \\ &\mathbf{s} = (s_1, s_2) = (\bar{\xi}, \bar{\eta}) \quad \text{for the source point} \end{aligned} \tag{26}$$

where

$$x_1 = c\cosh\xi\cos\eta, \quad x_2 = c\sinh\xi\sin\eta, \tag{27}$$

and

$$s_1 = c\cosh\bar{\xi}\cos\bar{\eta}, \quad s_2 = c\sinh\bar{\xi}\sin\bar{\eta}. \tag{28}$$

The fundamental solution, $U(\mathbf{s}, \mathbf{x})$, and kernel function $T(\mathbf{s}, \mathbf{x})$ in terms of degenerate (separable) kernel are shown below:

$$U(\mathbf{s}, \mathbf{x}) = \begin{cases} U^i(\bar{\xi}, \bar{\eta}; \xi, \eta) = \frac{1}{2\pi}\Big(\bar{\xi} + \ln\frac{c}{2} - \sum_{m=1}^{\infty}\frac{2}{m}e^{-m\bar{\xi}}\cosh m\xi\cos m\eta\cos m\bar{\eta} \\ \qquad\qquad - \sum_{m=1}^{\infty}\frac{2}{m}e^{-m\bar{\xi}}\sinh m\xi\sin m\eta\sin m\bar{\eta}\Big), \quad \bar{\xi} \geqslant \xi, \\ U^e(\bar{\xi}, \bar{\eta}; \xi, \eta) = \frac{1}{2\pi}\Big(\xi + \ln\frac{c}{2} - \sum_{m=1}^{\infty}\frac{2}{m}e^{-m\xi}\cosh m\bar{\xi}\cos m\eta\cos m\bar{\eta} \\ \qquad\qquad - \sum_{m=1}^{\infty}\frac{2}{m}e^{-m\xi}\sinh m\bar{\xi}\sin m\eta\sin m\bar{\eta}\Big), \quad \bar{\xi} < \xi, \end{cases} \tag{29}$$

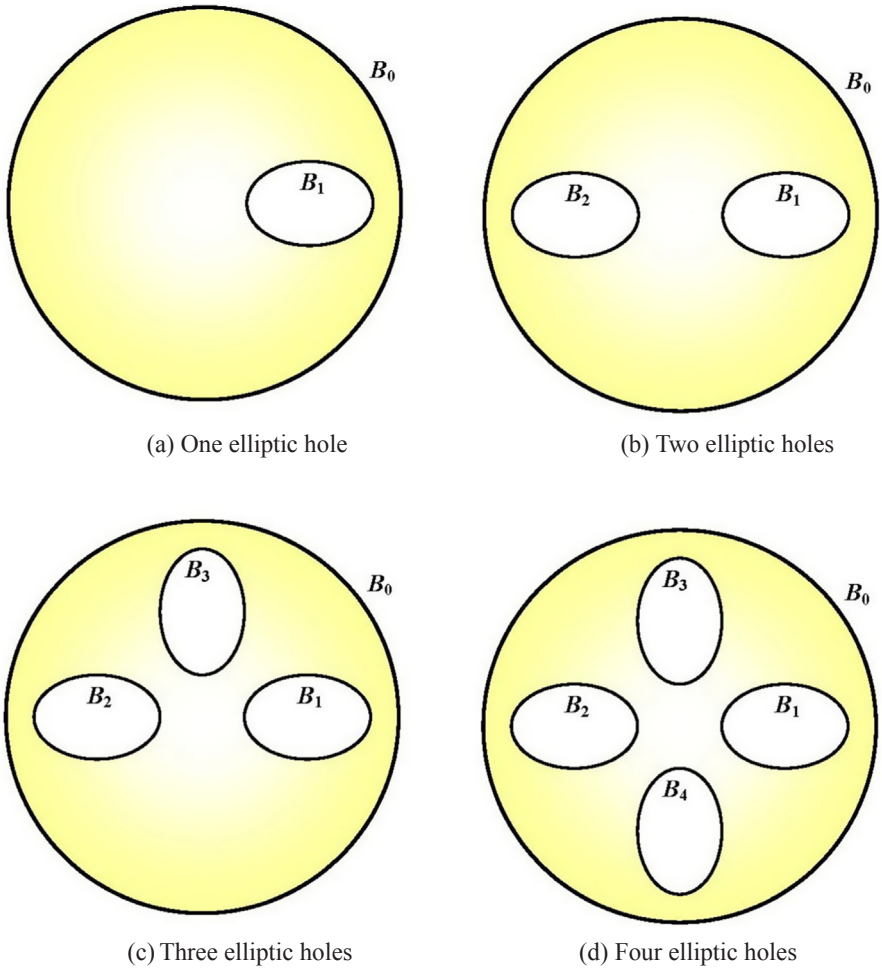

Fig. 5. A circular bar with one, two, three and four elliptic holes.

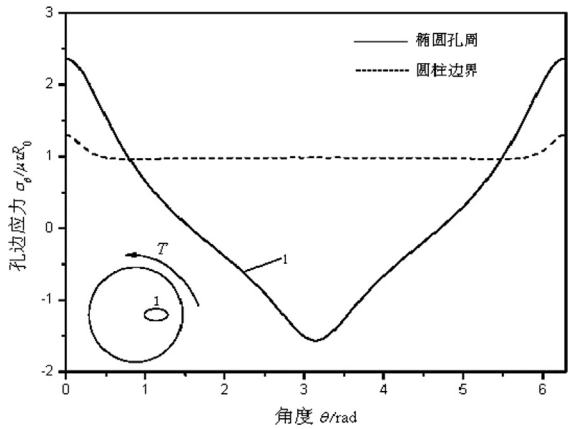

Fig. 6a. The stress around the boundary of the circular bar and the elliptic hole provided by Huang and Gao [17].

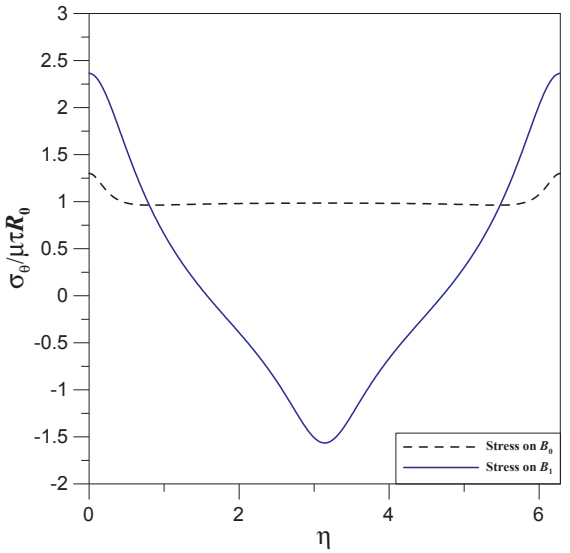

Fig. 6b. The stress around the boundary of the circular bar and the elliptic hole by using the proposed approach.

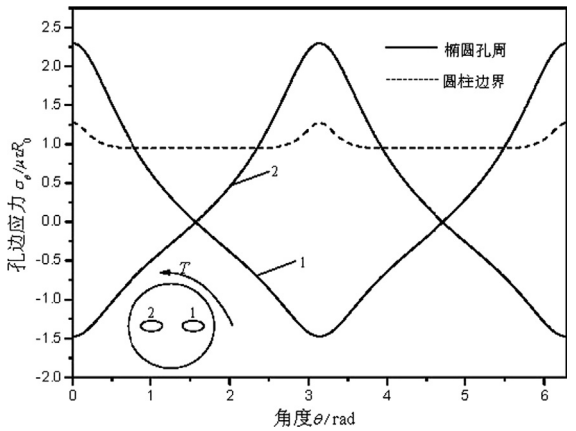

Fig. 7a. The stress around the boundary of the circular bar and two elliptic holes provided by Huang and Gao [17].

$$T(\mathbf{s},\mathbf{x})=\begin{cases} T^i(\bar{\xi},\bar{\eta};\xi,\eta)=\frac{1}{2\pi}\frac{1}{J_s}\Big(1+2\sum_{m=1}^{\infty}e^{-m\bar{\xi}}\cosh m\xi\cos m\eta\cos m\bar{\eta} \\ \qquad\qquad +2\sum_{m=1}^{\infty}e^{-m\bar{\xi}}\sinh m\xi\sin m\eta\sin m\bar{\eta}\Big), \quad \bar{\xi}\geqslant\xi, \\ T^e(\bar{\xi},\bar{\eta};\xi,\eta)=\frac{1}{2\pi}\frac{1}{J_s}\Big(-2\sum_{m=1}^{\infty}e^{-m\xi}\sinh m\bar{\xi}\cos m\eta\cos m\bar{\eta} \\ \qquad\qquad -2\sum_{m=1}^{\infty}e^{-m\xi}\cosh m\bar{\xi}\sin m\eta\sin m\bar{\eta}\Big), \quad \bar{\xi}<\xi, \end{cases} \tag{30}$$

where superscripts "i" and "e" denote the interior ($\bar{\xi}\geqslant\xi$) and exterior ($\bar{\xi}<\xi$) cases, respectively. The other kernels $L(\mathbf{s},\mathbf{x})$ and $M(\mathbf{s},\mathbf{x})$ in the boundary integral equation can be obtained by utilizing the operators of Eq. (13) with respect to the kernel $U(\mathbf{s},\mathbf{x})$. In the real implementation, the degenerate kernel can be expressed as finite sums of products of functions of $\mathbf{s}$ alone and functions of $\mathbf{x}$ alone. It is worthy of noting that the limiting scheme of approaching the radial coordinate ($\bar{\xi}$ or ξ) to zero is used to simulate line cracks.

For the kth boundary densities, we apply the eigenfunction expansions to approximate the potential $\varphi(\mathbf{s})$ and its normal derivative $\psi(\mathbf{s})$ on the elliptic boundary as follows:

$$\varphi(\mathbf{s})=a_0+\sum_{n=1}^{\infty}a_n\cos n\bar{\eta}+\sum_{n=1}^{\infty}b_n\sin n\bar{\eta}, \tag{31}$$

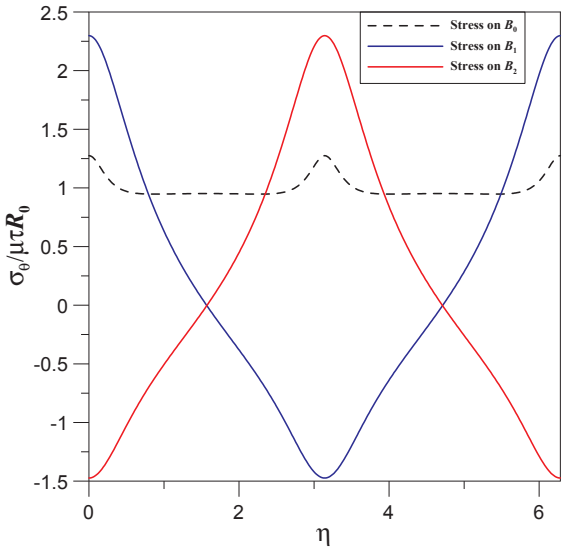

Fig. 7b. The stress around the boundary of the circular bar and two elliptic holes by using the proposed approach.

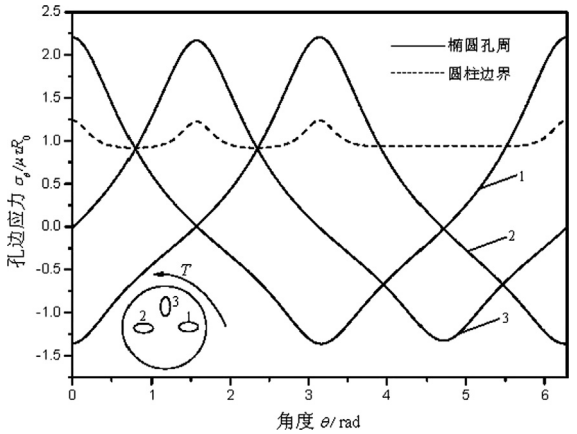

Fig. 8a. The stress around the boundary of the circular bar and three elliptic holes provided by Huang and Gao [17].

$$\psi(\mathbf{s}) = \frac{1}{J_s}\left(p_0 + \sum_{n=1}^{\infty} p_n \cos n\bar{\eta} + \sum_{n=1}^{\infty} q_n \sin n\bar{\eta}\right), \tag{32}$$

where a_0, a_n, b_n, p_0, p_n and q_n are the coefficients of the eigenfunction expansions, $\bar{\eta}$ is the angle ($0 \leqslant \theta < 2\pi$) and J_s is the Jacobian with respect to the source point and the definition is

$$J_s(\bar{\xi}, \bar{\eta}) = c\sqrt{(\sinh\bar{\xi}\cos\bar{\eta})^2 + (\cosh\bar{\xi}\sin\bar{\eta})^2}. \tag{33}$$

Here, it can be observed that the terms of J_s which may exist in the degenerate kernel, boundary density and boundary integral are cancelled out each other naturally in the boundary integration. Therefore, the elliptic integral is not required to deal with. In the real computation, only the finite M number of terms is used in the summation. The present method belongs to one kind of semi-analytical methods since error only attributes to the number of truncation term of the eigenfunction expansions.

2.2.4. Linear algebraic system

In order to calculate the unknown coefficients, $2M + 1$ boundary nodes for each circular boundary, elliptic boundary or crack are needed. After locating the null-field point $\mathbf{x}_k$ exactly on the kth circular boundary, elliptic boundary or crack in Eqs. (20) or (24), we have

$$0 = \sum_{j=0}^{N} \int_{B_j} T(\mathbf{s}, \mathbf{x})\varphi(\mathbf{s})dB_j(s) - \sum_{j=0}^{N} \int_{B_j} U(\mathbf{s}, \mathbf{x})\psi(\mathbf{s})dB_j(\mathbf{s}), \quad \mathbf{x} \in \Omega^c \cup B, \tag{34}$$

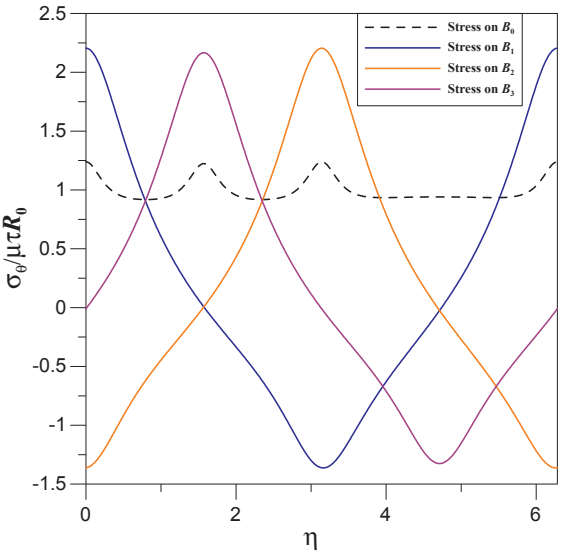

Fig. 8b. The stress around the boundary of the circular bar and three elliptic holes by using the proposed approach.

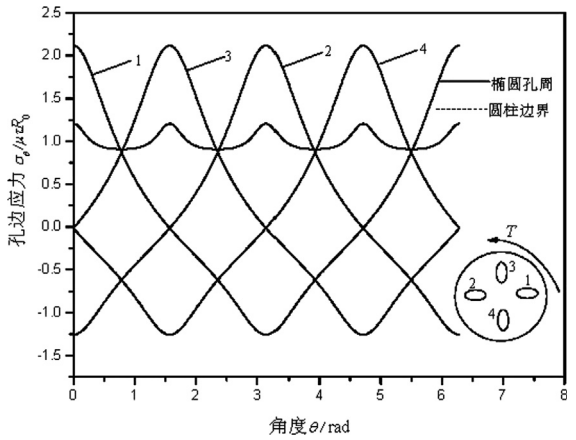

Fig. 9a. The stress around the boundary of the circular bar and four elliptic holes provided by Huang and Gao [17].

where N is the number of holes and cracks. Since the boundary integral equations are frame indifferent, *i.e.*, objectivity rule is satisfied. The origin of observer system is adaptively chosen at the center of circular boundary, elliptic boundary or crack under integration. The term $dB_j(s)$ in the integral equation denotes the jth boundary integration for the source density. Therefore, the origin is set up at the center of the jth elliptic boundary. When $\mathbf{x}$ is located on the kth boundary, the position parameter (ξ, η) can be determined by the origin in the jth elliptic boundary. For this reason, $\mathbf{x} = (\xi, \eta)$ depends on the origin of observer system. They are determined by the origin of elliptic boundary which you intend to integrate. This is the so-called adaptive observer system [4,7]. For B_j integral of the jth boundary, the kernels of $U(\mathbf{s}, \mathbf{x})$ and $T(\mathbf{s}, \mathbf{x})$ are expressed in terms of degenerate kernels, and $\varphi(\mathbf{s})$ and $\psi(\mathbf{s})$ are substituted by using the eigenfunction expansions. For simplicity, a linear algebraic system is obtained

$$[\mathbf{U}]\{\psi\} = [\mathbf{T}]\{\varphi\}, \tag{35}$$

where $[\mathbf{U}]$ and $[\mathbf{T}]$ are the influence matrices with a dimension of $(N + 1) \times (2M + 1)$ by $(N + 1) \times (2M + 1)$, $\{\varphi\}$ and $\{\psi\}$ denote the column vectors of Fourier and eigenfunction coefficients with a dimension of $(N + 1) \times (2M + 1)$ by 1 in which $[\mathbf{U}]$, $[\mathbf{T}]$, $\{\varphi\}$ and $\{\psi\}$ can be defined as follows:

$$[\mathbf{U}] = \begin{bmatrix} \mathbf{U}_{00} & \mathbf{U}_{01} & \cdots & \mathbf{U}_{0N} \\ \mathbf{U}_{10} & \mathbf{U}_{11} & \cdots & \mathbf{U}_{1N} \\ \vdots & \vdots & \ddots & \vdots \\ \mathbf{U}_{N0} & \mathbf{U}_{N1} & \cdots & \mathbf{U}_{NN} \end{bmatrix}, \tag{36}$$

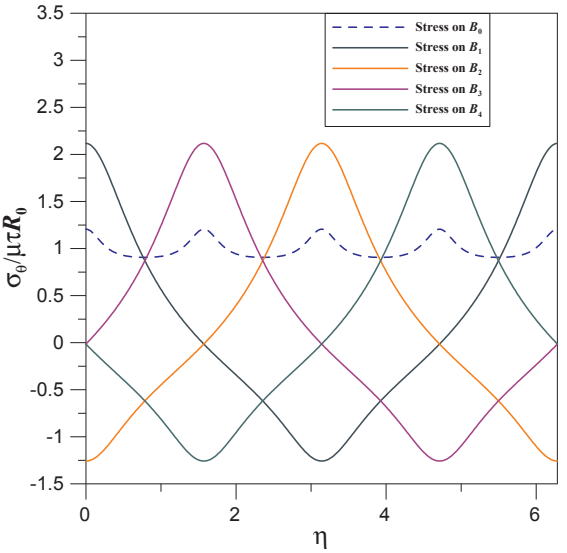

Fig. 9b. The stress around the boundary of the circular bar and four elliptic holes by using the proposed approach.

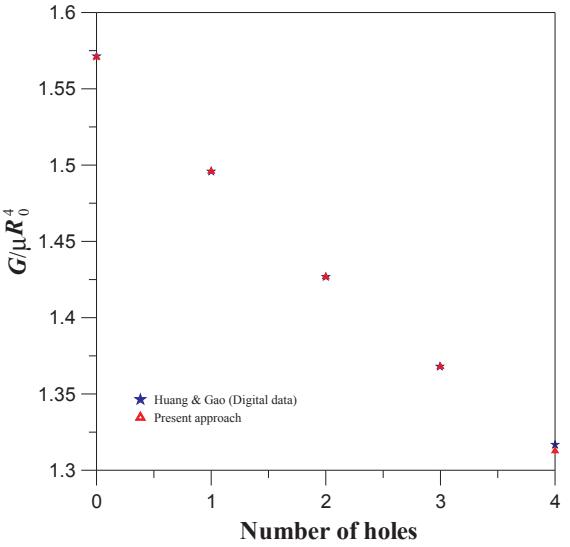

Fig. 10. The torsional rigidity versus the number of elliptic holes.

$$[\mathbf{T}] = \begin{bmatrix} \mathbf{T}_{00} & \mathbf{T}_{01} & \cdots & \mathbf{T}_{0N} \\ \mathbf{T}_{10} & \mathbf{T}_{11} & \cdots & \mathbf{T}_{1N} \\ \vdots & \vdots & \ddots & \vdots \\ \mathbf{T}_{N0} & \mathbf{T}_{N1} & \cdots & \mathbf{T}_{NN} \end{bmatrix}, \tag{37}$$

$$\{\varphi\} = \begin{Bmatrix} \varphi_0 \\ \varphi_1 \\ \varphi_2 \\ \vdots \\ \varphi_N \end{Bmatrix}, \quad \{\psi\} = \begin{Bmatrix} \psi_0 \\ \psi_1 \\ \psi_2 \\ \vdots \\ \psi_N \end{Bmatrix}, \tag{38}$$

where the vectors $\{\varphi_k\}$ and $\{\psi_k\}$ are in the forms of $\{a_0^k\ a_1^k\ b_1^k \cdots a_M^k\ b_M^k\}^T$ and $\{p_0^k\ p_1^k\ q_1^k \cdots p_M^k\ q_M^k\}^T$, respectively; the first subscript "j" ($j = 0,\ 1,\ \cdots, N$) in $[\mathbf{U}_{jk}]$ and $[\mathbf{T}_{jk}]$ denotes the index of the jth boundary where the observation point is located and the second subscript "k" ($k = 0,\ 1,\ \cdots, N$) denotes the index of the kth boundary where the boundary data $\{\varphi_k\}$ and $\{\psi_k\}$ are specified and M indicates the number of truncated terms of the eigenfunction expansions. In Eq. (35), $\{\psi\}$ is the input data from the boundary condition and $\{\varphi\}$ is the unknown data to be determined. The flowchart of the proposed approach is shown in Fig. 4.

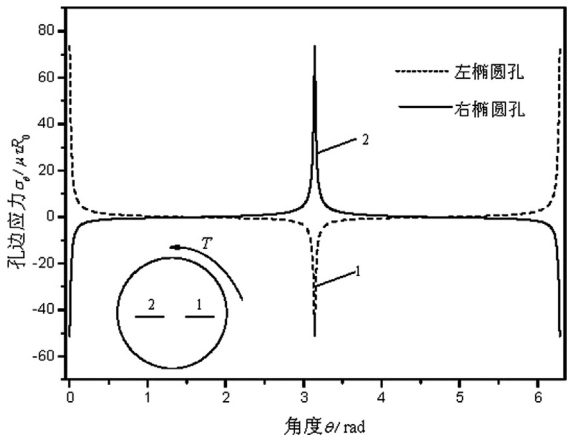

Fig. 11a. The stress around two elliptic holes provided by Huang and Gao [17] ($b = 0.002R_0$).

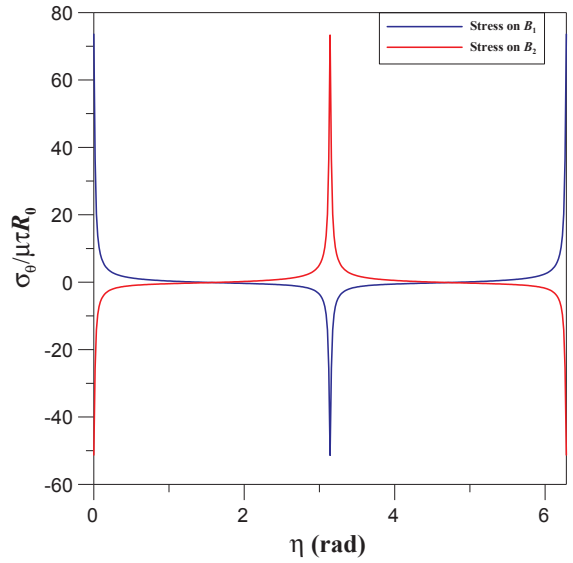

Fig. 11b. The stress around two elliptic holes by using the proposed approach ($b = 0.002R_0$).

3. Numerical examples

In order to show the feasibility and validity of the proposed approach, we use several numerical examples to compare with our approach. In the following numerical example, the radius (R_0) of the circular bar is given 6. In our program, the lengths of semi-major and semi-minor axis are respectively given 6.000001 and 6 to approximate a circular bar. The other parameters are given in each numerical example.

3.1. Example 1: A circular bar with multiple elliptic holes

In the first example, we consider a circular bar with one, two, three and four elliptic holes as shown in Fig. 5. The semi-major and semi-minor axes of elliptic holes are given $0.2R_0$ and $0.1R_0$, respectively. The eccentricity of each elliptic hole is $0.6R_0$. Here, we study the effects of increasing the number of elliptic holes for the torsional rigidity and stress. The stress around the boundary of circular bar and elliptic holes are shown in Figs. 6–9. After comparing our results with Haung and Gao's results [17], good agreements are made. In Figs. 6–9, it is found that the peak of the stress around the elliptic holes slightly decreases when the number of elliptic holes is increased. Besides, we also determine the torsional rigidity by using the following formula

$$G = \int_D (x^2 + y^2)dD - \sum_{k=1}^{N} \int_{B_k} \varphi \frac{\partial \varphi}{\partial n} dB_k. \tag{39}$$

The torsional rigidity versus the number of elliptic holes is shown in Fig. 10. Since the numerical data are not provided in Huang

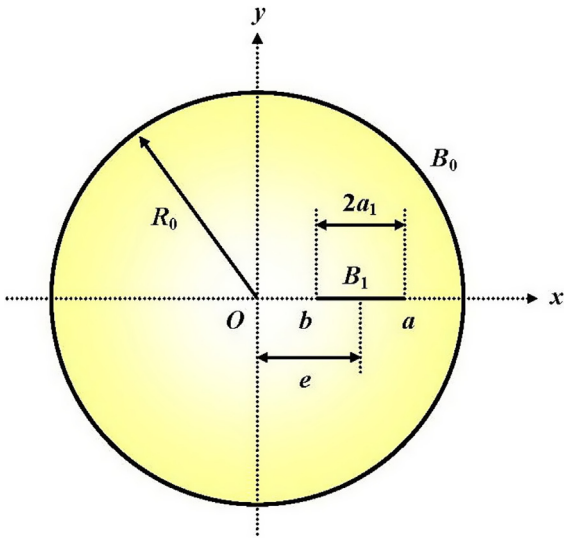

Fig. 12. A circular bar with a single crack.

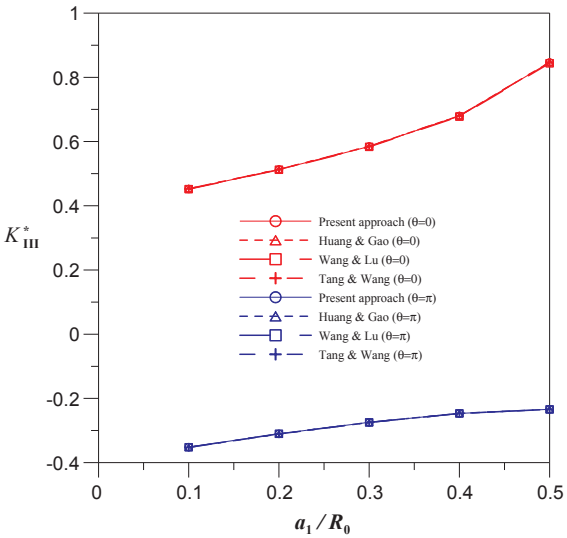

Fig. 13. The nondimensional stress intensity factor versus various ratios of a_1/R_0 for a circular bar with a single crack.

and Gao's paper [17], the digitizing technique is employed to capture the data for comparison. As shown in Fig. 8, our results agree well with Huang and Gao's results when the number of elliptic holes is equal to 1, 2 and 3. Although there is a little deviation (relative error less than 0.4%) for the case of four holes, this is an acceptable result. Besides, it is found that the torsional rigidity gradually decreases following the increase of the number of holes. In order to show effect of the ratio of the semi-major and semi-minor axes, we fix the lengths of semi-major axis ($a_1 = a_2 = 0.2R_0$) for the case of two elliptic holes and give the lengths of semi-minor axis, $b_1 = b_2 = 0.002R_0$. The stresses around the two elliptic holes are shown in Fig. 11. Our results match well with those of Huang and Gao [17] as shown in Figs. 11a and 11b. Obviously, when the ratio of the semi-major and semi-minor axes becomes much smaller, we can easily observe the phenomena of stress concentration on the holes.

3.2. Example 2: A circular bar with line cracks

3.2.1. Case 1: A circular bar with single crack

The case considered here is a circular bar with a crack as shown in Fig. 12. This problem has been discussed by Wang and Lu [15] and Haung and Gao [17]. Besides, for comparison, Wang and Lu [15] also provided the results by using the Gauss-Chebyshev integration formulas which was proposed by Tang and Wang [32]. In this case, the non-dimensional eccentric length (d/R_0) is 0.4. Here, we give a small length of the semi-minor axis ($b_1 = 0.001$) to simulate an elliptic hole as a crack. Not only torsional rigidities but also the non-dimensional stress intensity factors (SIF) are calculated. Based on Huang and Gao [17], the formula of non-dimensional

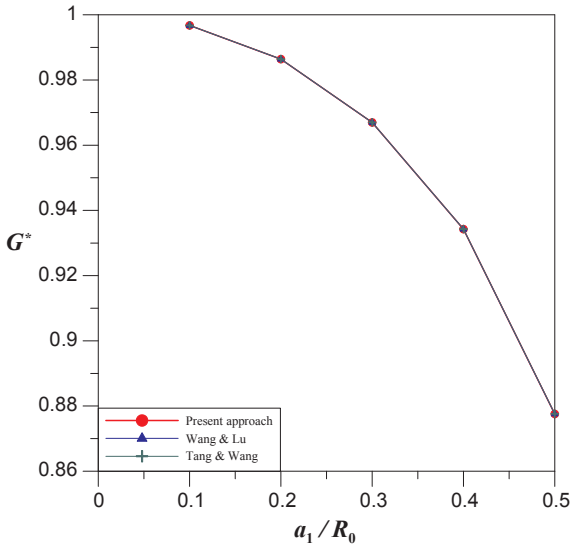

Fig. 14. The nondimensional torsional rigidity versus various ratios of a_1/R_0 for a circular bar with a single crack.

Table 1
Non-dimensional stress intensity factor and torsional rigidity versus the ratio of a_1/R_0 of crack.

$\frac{a_1}{R_0}$	K^*_{III} $(\theta = 0)$				K^*_{III} $(\theta = \pi)$				Torsional rigidity G^*		
	Tang and Wang [32]	Wang and Lu [15]	Huang and Gao [17]	Present	Tang and Wang [32]	Wang and Lu [15]	Huang and Gao [17]	Present	Tang and Wang [32]	Wang and Lu [15]	Present
0.1	0.4530	0.4519	0.4530	0.4520	−0.3527	−0.3521	−0.3527	−0.3518	0.996752	0.996751	0.996747
0.2	0.5133	0.5120	0.5133	0.5129	−0.3109	−0.3104	−0.3109	−0.3104	0.986411	0.986407	0.986399
0.3	0.5851	0.5834	0.5851	0.5848	−0.2749	−0.2747	−0.2749	−0.2746	0.967002	0.966991	0.966981
0.4	0.6801	0.6780	0.6801	0.6798	−0.2469	−0.2469	−0.2469	−0.2467	0.934280	0.934257	0.934246
0.5	0.8469	0.8439	0.8469	0.8465	−0.2342	−0.2344	−0.2342	−0.2340	0.877602	0.877553	0.877550

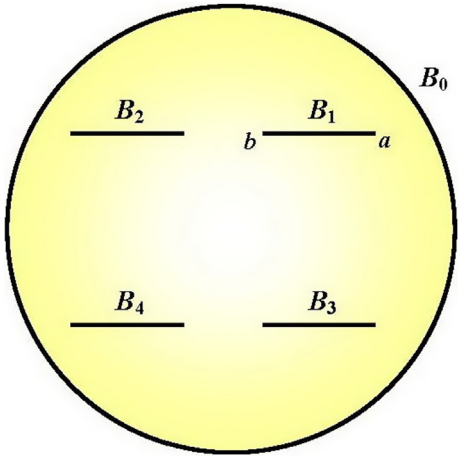

Fig. 15. A circular bar with four identical cracks of parallel distribution.

stress intensity factors is given below:

$$K^*_{III} = \frac{K_{III}}{\mu\alpha R_0 \sqrt{a_1}} \tag{40}$$

where K_{III} is defined as follows:

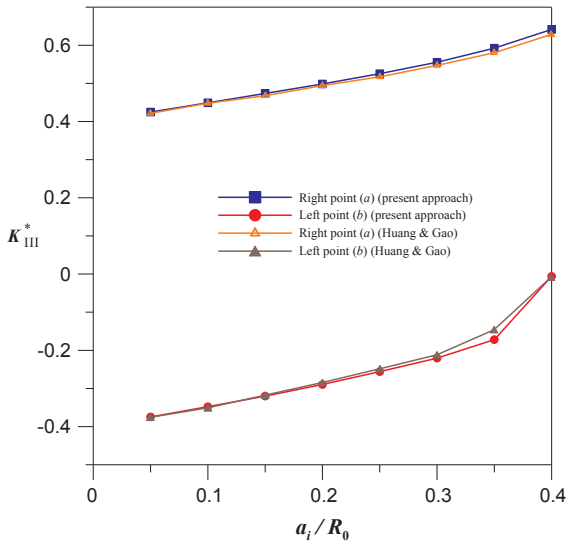

Fig. 16. The nondimensional stress intensity factor versus various ratios of a_i/R_0 for the case of four identical cracks.

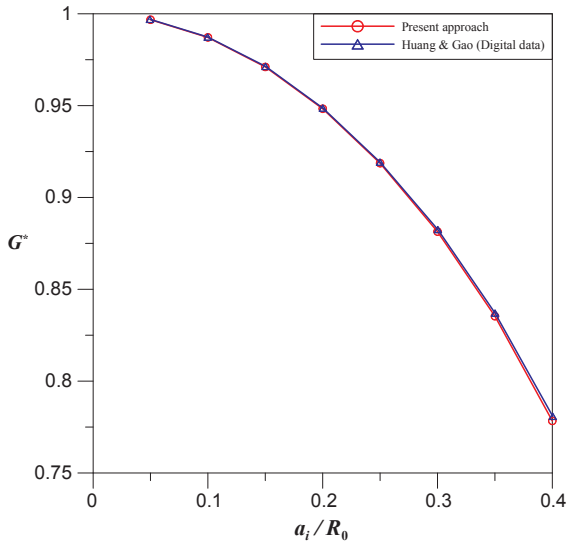

Fig. 17. The nondimensional torsional rigidity versus various ratios of a_i/R_0 for the case of four identical cracks.

$$K_{III} = \lim_{\rho \to 0} \sqrt{2\rho}\ \tau_{\theta z} \tag{41}$$

in which ρ is the radial coordinate of crack tip. In the real computation, the value of K_{III} is evaluated from an extremely small value for ρ and an extremely large value for $\tau_{\theta z}$. Also, the nondimensional torsional rigidity is defined as

$$G^* = \frac{2G}{\pi \mu R_0^4}. \tag{42}$$

The nondimensional stress intensity factor and torsional rigidity versus various ratio of a_1/R_0 of crack are shown in Figs. 13 and 14, respectively. Besides, all the data are also given in Table 1. After comparing our results with those of Tang and Wang [32], Wang and Lu [15] and Haung and Gao [17], good agreements not only for stress intensity factor but also for torsional rigidity are made.

3.2.2. Case 2: A circular bar with four identical cracks of parallel distribution

In Fig. 15, a circular bar with four identical cracks of parallel distribution is considered. In this case, the centers of four elliptic holes are set at $(\pm 0.4R_0, \pm 0.4R_0)$. The lengths of semi-major axis $(a_1 = a_2 = a_3 = a_4 = a_i)$ and semi-minor axis $(b_1 = b_2 = b_3 = b_4 = 0.001)$ are used to approximate the four cracks. Here, we study the effect of various ratios of crack length (a_i/R_0) for the torsional rigidity and stress intensity factor as shown in Figs. 16 and 17. We also compare our results with those of Haung and

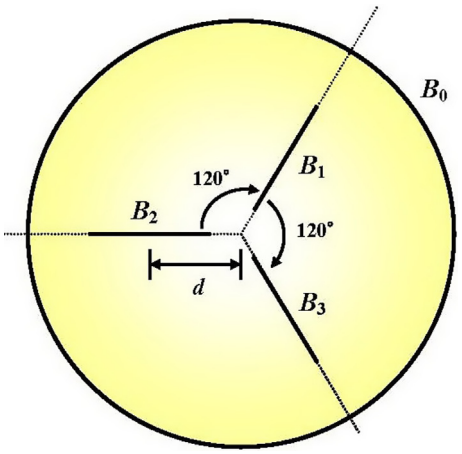

Fig. 18. A circular bar with three identical cracks of radial distribution.

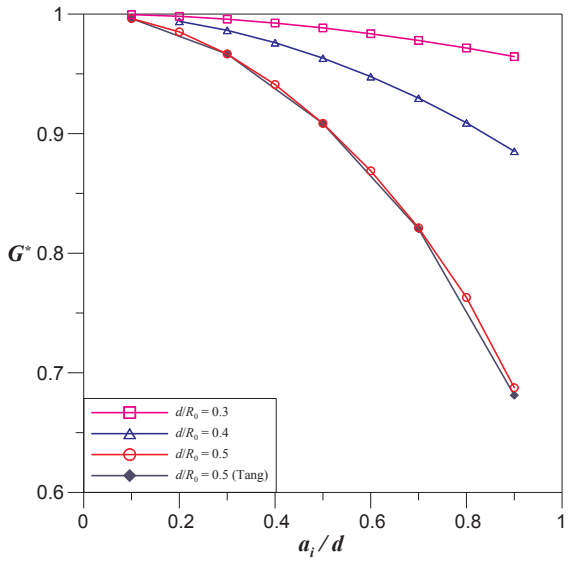

Fig. 19. The nondimensional torsional rigidity versus various crack length for the case of three identical cracks of radial distribution.

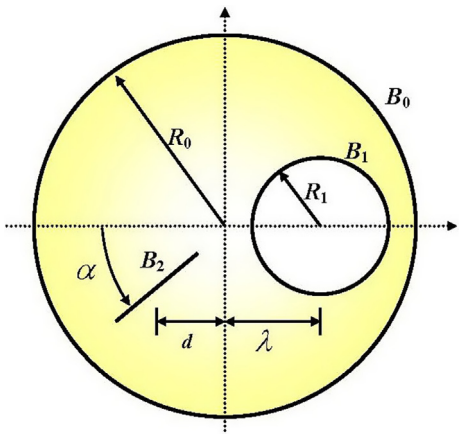

Fig. 20. A circular bar with a circular hole and a radial crack.

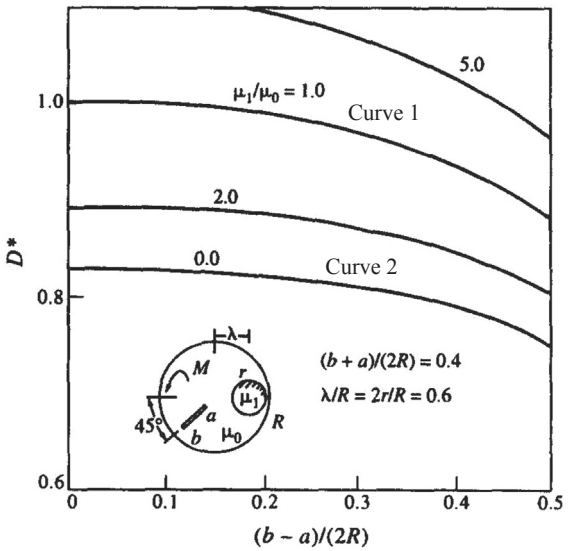

Fig. 21a. The nondimensional torsional rigidity versus various crack length provided by Yue and Tang [14].

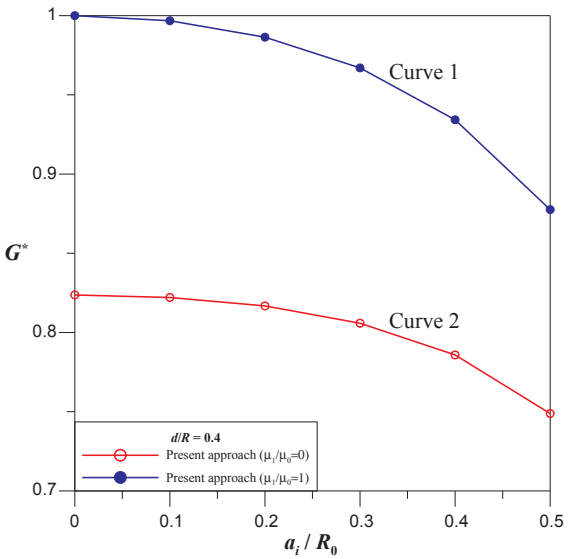

Fig. 21b. The nondimensional torsional rigidity versus various crack length by using the proposed approach.

Gao [17]. The acceptable results are obtained by using the proposed approach. As the same results of the foregoing case, when the length of the crack increases, the torsional rigidity gradually becomes small. Besides, the stress intensity factor at the crack tip near the outer boundary becomes large and the one near the center of the bar becomes small. These phenomena also appear in [17].

3.2.3. *Case 3: A circular bar with three identical cracks of radial distribution*

The torsion problem is considered here for a circular bar with three identical cracks ($a_1 = a_2 = a_3 = a_i$) of radial distribution as shown in Fig. 18. In this case, the lengths of semi-minor axis are given $b_1 = b_2 = b_3 = 0.001$ and we study the effect of the non-dimensional torsional rigidity versus various crack length as shown in Fig. 19. Since the available data in [13] is $\frac{a_i}{d} = 0.1,\ 0.3,\ 0.5,\ 0.7,\ 0.9$ for the case of $\frac{d}{R_0} = 0.5$, it is found that our results match well with those except for the point of $\frac{a_i}{d} = 0.9$. However, the relative error at this point is about 1%. This is also an acceptable result.

3.3. *Example 3: A circular bar with a circular hole and a radial crack*

The configuration of a circular bar with a circular hole and a crack solved here is shown in Fig. 20. In this case, the parameters are given as $\alpha = \frac{\pi}{4}$, $\frac{d}{R_0} = 0.4$ and $\frac{\lambda}{R_0} = \frac{2R_1}{R_0} = 0.6$. Yue and Tang [14] have studied the composite circular bar with a radial crack. In their

work, they discussed the effect of different crack length and various ratio of $\frac{\mu_1}{\mu_0}$ for a circular bar. However, for $\frac{\mu_1}{\mu_0} = 0$ and $\frac{\mu_1}{\mu_0} = 1$, they can be seen as two different special cases. One is a circular bar with a circular hole and a crack $\left(\frac{\mu_1}{\mu_0} = 0\right)$, and the other $\left(\frac{\mu_1}{\mu_0} = 1\right)$ is a circular bar with a crack. Due to the same material $\left(\frac{\mu_1}{\mu_0} = 1\right)$, it means that the shear modulus of the bar is same as the circular inclusion. It indicates that the bar and the inclusion are the same material. This has been solved in the case 1 of Example 2 by using the proposed approach. The nondimensional torsional rigidity versus the crack length proposed by Yue and Tang [14] is shown in Fig. 21a. Results of the proposed approach subject to $\frac{\mu_1}{\mu_0} = 0$ and $\frac{\mu_1}{\mu_0} = 1$ are given in Fig. 21b. The trend of the curves is similar to those of Yue and Tang [14]. In the table of reference [14], they gave the nondimensional torsional rigidity $D^* = 0.967$, the nondimensional stress intensity factor $K^*_{III}(b) = 0.60502$ and $K^*_{III}(a) = 0.28425$ for the case of $\frac{\mu_1}{\mu_0} = 1$ and $\frac{a_1}{R_0} = 0.3$. The value of nondimensional torsional rigidity is the same as the data in Table 1. However, the nondimensional stress intensity factor is larger than those in Table 1.

4. Conclusions

In this paper, we have proposed a semi-analytical approach of using the null-field integral equation in conjunction with the degenerate kernel and eigenfunction expansion to solve torsion problems of a circular bar with holes and/or cracks. The proposed approach different from the conventional boundary element method is that we don't need to calculate the principal value. Besides, only the observation points are distributed on the real boundary to match boundary conditions and the unknown coefficients can be easily determined from a linear algebraic system. Therefore, the proposed approach can be seen as one kind of meshless methods. Furthermore, in our formulation, only the *UT* formulation is used to solve the problem and we don't need to separate to two subdomains when the solved problem contains the crack. Through the limiting processes of numerically approaching the length of semi-major axis to the length of semi-minor axis (to approximate the circular geometry) and numerically making the length of semi-minor axis close to zero (to simulate line crack), the proposed approach can deal with problems containing the circular geometry and line crack as the special case of elliptic boundary. Finally, a general program was developed for solving a circular torsion bar with circular and elliptic holes and/or cracks. Several numerical examples were also given to show the validity of the proposed approach. Good agreements are made after comparing with the available results in the literature.

Acknowledgements

This work was supported by the Ministry of Science and Technology [grant numbers MOST 103-2221-E-019-011 and MOST107-2221-E-019-006] for National Taiwan Ocean University.

References

[1] Ling CB. Torsion of a circular tube with longitudinal circular holes. Q Appl Math 1947;5:168–81.
[2] Muskhelishvili NI. Some basic problems of the mathematical theory of elasticity. Groningen: P. Noordhoff; 1963.
[3] Chen T, Weng IS. Torsion of a circular compound bar with imperfect interface. J Appl Mech 2001;68:955–8.
[4] Caulk DA. Analysis of elastic torsion in a bar with circular holes by a special boundary integral method. J Appl Mech 1983;50:101–8.
[5] Katsikadelis JT, Sapountzakis EJ. Torsion of composite bars by boundary element method. J Eng Mech 1985;111:1197–210.
[6] Sapountzakis EJ, Mokos VG. Nonuniform torsion of composite bars by boundary element method. J Eng Mech 2001;127:945–53.
[7] Sapountzakis EJ, Mokos VG. Warping shear stresses in nonuniform torsion of composite bars by BEM. Comput Meth Appl Mech Eng 2003;192:4337–53.
[8] Sapountzakis EJ, Mokos VG. Nonuniform torsion of composite bars of variable thickness by BEM. Int J Solids Struct 2004;41:1753–71.
[9] Shams-Ahmadi M, Chou SI. Complex variable boundary element method for torsion of composite shafts. Int J Numer Methods Eng 1997;40:1165–79.
[10] Ang WT, Kang I. A complex variable boundary element method for elliptic partial differential equations in a multiply-connected region. Int J Comput Math 2000;75:515–25.
[11] Petrov EP. Analysis of torsion and shear characteristics of beam cross-sections by the boundary element method. Int J BEM Commun 1997;8:239–45.
[12] Sih GC. Stress distribution near internal crack tips for longitudinal shear problems. J Appl Mech 1965;32:51–8.
[13] Tang RJ. Torsion theory of the crack cylinder. Shanghai: Shanghai Jiao Tong University Publisher; 1996. [in Chinese].
[14] Yue JC, Tang RJ. Integral equation method for the torsion of a composite cylinder with crack and inclusion. Eng Fract Mech 1996;55:763–75.
[15] Wang YB, Lu ZZ. New boundary element method for torsion problems of a cylinder with curvilinear cracks. Appl Math Mech 2005;26:1387–93. [in Chinese].
[16] Lu ZZ, Wang YB, Chen LZ, Xu JQ. A new boundary method for torsion problems of bars with curvilinear cracks. Eng Mech 2007;24:41–6. [in Chinese].
[17] Huang C, Gao CF. Torsion of circular shaft containing multiple elliptical holes or cracks. Eng Mech 2011;28:28–34. [in Chinese].
[18] Jin B. A meshless method for the Laplace and biharmonic equations subjected to noisy boundary data. Comput Model Eng Sci 2004;6:253–62.
[19] Sladek V, Sladek J, Tanaka M. Local integral equations and two meshless polynomial interpolations with application to potential problems in non-homogeneous media. Comput Model Eng Sci 2005;7:69–84.
[20] Chen JT, Shen WC, Chen PY. Analysis of circular torsion bar with circular holes using null-field approach. Comput Model Eng Sci 2006;12:109–19.
[21] Bird MD, Steele CR. Separated solution procedure for bending of circular plates with circular holes. J Appl Mech 1991;59:398–404.
[22] Naghdi AK. Bending of a perforated circular cylindrical cantilever. Int J Solids Struct 1991;28:739–49.
[23] Chen JT, Chen PY. A semi-analytical approach for stress concentration of cantilever beams with holes under bending. J Mech 2007;23:211–21.
[24] Chen JT, Lee YT. Torsional rigidity of a circular bar with multiple circular inclusions using the null-field integral approach. Comput Mech 2009;44:221–32.
[25] Kuo YM, Conway HD. The torsion of composite tubes and cylinders. Int J Solids Struct 1973;9:1553–65.
[26] Murakami H, Yamakawa J. Torsional wave propagation in reinforced concrete columns. Int J Solids Struct 1998;35:2617–37.
[27] Chen JT, Lee YT, Lee JW. Torsional rigidity of an elliptic bar with multiple elliptical inclusions using a null-field integral approach. Comput Mech 2010;46:511–9.
[28] Timoshenko SP, Goodier JN. Theory of elasticity. New York: McGraw-Hill; 1970.
[29] Chen YZ, Lin XY. Dual boundary integral equation formulation in antiplane elasticity using complex variable. Comput Mech 2010;45:167–78.
[30] Chen YZ, Lin XY. Dual boundary integral equation formulation in plane elasticity using complex variable. Eng Anal Bound Elem 2010;34:834–44.
[31] Chen YZ. Numerical solution of the t-version complex variable boundary integral equation for the interior region in plane elasticity. Eng Anal Bound Elem 2014;46:75–84.
[32] Tang RJ, Wang YB. On the problem of crack system with an elliptic hole. Acta Mech Sinica 1986;2:47–57.